

TiO₂ nanotube formation by Ti film anodization and their transport properties for dye-sensitized solar cells

Masoud Iraj¹ · Mohammadreza Kolahdouz¹ · Ebrahim Asl-Soleimani¹ ·
Emad Esmaeili¹ · Zahra Kolahdouz²

Received: 22 December 2015 / Accepted: 9 February 2016
© The Author(s) 2016. This article is published with open access at Springerlink.com

Abstract In this paper, we present the synthesis of TiO₂ nanotube (NT) arrays formed by anodization of Ti film deposited on a fluorine-doped tin oxide-coated glass substrate by direct current magnetron sputtering. NH₄F/ethylene glycol electrolyte was used to demonstrate the growth of stable nanotubes at room temperature. TiO₂ NTs as long as 4.8 μm with the high expansion factor to the initial sputtered Ti film (2 μm) were obtained, showing little undesired dissolution of the metal in the electrolyte during anodization. The average pore size and wall thickness of NTs were about 70 and 30 nm, respectively. Structural investigations on the transparent NT arrays reveal the presence of anatase phase after annealing. The NTs were sensitized by the N719 complex and the resultant photoelectrodes were incorporated into dye sensitized solar cells (DSSCs). The conversion efficiency of 1.97 % was obtained under AM 1.5 illumination and the open circuit voltage, short circuit current density and the fill factor were 0.59 V, 6.71 mA/cm² and 0.50, respectively. Investigation of the electron transport of the DSSCs by electrochemical impedance spectroscopy showed that the electron diffusion length (8.6 μm) was higher than NTs' height. It was also observed that the electron transport resistance measured in

NT DSSC was lower compared to the reported TiO₂ nanoparticle one.

1 Introduction

Titanium dioxide nanotubes have proven to be a highly promising material for application in various fields, such as sensing, photocatalysis and photovoltaics [1–3]. For instance, when used as one-dimensional nanostructure photoanodes in dye-sensitized solar cells (DSSCs), they were found to show higher light harvesting and charge-collection efficiencies compared to their nanoparticle-based counterparts owing to their faster electron transport and slower charge recombination properties [4, 5].

A suitable method for fabrication of TiO₂ nanotubes is anodization of metallic Ti. Commonly, high purity Ti foils are used and anodized in aqueous HF-containing solutions or non-aqueous electrolytes containing fluoride ions [6, 7]. However, especially for photovoltaic devices, TiO₂ nanotubes on conducting glass are of particular interest. Structures on conducting glass substrates allow front side illumination, i.e. illumination from the substrate side, resulting in reduced loss of incident light intensity compared to cells fabricated from foils [8].

In this study, we fabricated an anodic TiO₂ nanotube film on a transparent conductive oxide (TCO) layer by anodization of a sputtered Ti film in an ethylene glycol solution of ammonium fluoride (NH₄F). The structure and morphology of prepared samples were characterized by X-ray diffraction and field emission scanning electron microscopy (FESEM). Finally, the photovoltaic performance of the prepared sample as the DSSC photoanode was investigated and the electron transport and

✉ Mohammadreza Kolahdouz
kolahdouz@ut.ac.ir

✉ Zahra Kolahdouz
z.kolahdouzesfahani@tudelft.nl

¹ School of Electrical and Computer Engineering, University of Tehran, Tehran, Islamic Republic of Iran

² Delft Institute of Microsystems and Nanoelectronics (DIMES), Delft University of Technology, Delft, The Netherlands

recombination properties of TiO₂ NTs were characterized using electrochemical impedance spectroscopy (EIS).

2 Experimental details

2.1 Deposition of Ti films on FTO substrate

The 2 μm titanium films were deposited on FTO coated glass (TEC-15, 15 ohm per square) using DC magnetron sputtering from a 99.99 % pure titanium target. The sputtering chamber was pumped down to the pressure of 2×10^{-3} mTorr before argon gas was introduced. Sputtering was operated in pure argon (23 sccm) and the working pressure was kept at 1.3 mTorr with the cathode power of 100 W. The substrate temperature was 300 °C, and the deposition time was about 150 min.

2.2 Preparation of TiO₂ nanotube arrays on FTO substrate by anodization

TiO₂ nanotube arrays were fabricated via electrochemical anodization in a two-electrode cell setup using $1.5 \times 1 \text{ cm}^2$ sample of Ti sputtered FTO/glass as a working electrode and stainless steel foil as the counter electrode. Anodization was performed in the ethylene glycol based electrolyte solution containing NH₄F (0.5 wt%) at 50 V. The resulting TiO₂ nanotubes on the FTO substrate were rinsed with DI water and ethanol, and then dried in air. Anatase TiO₂ was obtained by annealing the anodized samples at 450 °C for 30 min, in air ambient.

2.3 Dye sensitized solar cell fabrication

The DSSCs were fabricated by soaking the nanotube array films in 0.4 mM N719 dye (Solaronix) in acetonitrile for 20 h. Counter electrode was prepared by deposition of Pt on FTO/glass by coating with a drop of H₂PtC₁₆ solution (5 mM in isopropyl alcohol) with repetition of the heat treatment at 400 °C for 15 min. The dye-covered TiO₂ electrode and Pt-counter electrode were assembled into a sandwich type cell and sealed with 30 μm surlyn (Dyesol) spacer which was annealed at 120 °C for a few seconds. The cells were filled with a redox electrolyte (I⁻/I₃⁻).

2.4 Sample characterization and device measurements

The crystal structure and morphology of as-grown TiO₂ nanorods were investigated by X-ray diffraction (XRD) on a Philips X'pert Pro (the Netherlands) using Cu-K α radiation ($\lambda = 1.54 \text{ nm}$), and field emission scanning electron microscopy (FESEM, Hitachi S-4160).

Photovoltaic measurements were performed using simulated AM 1.5 sunlight with an output power of 100 mW/cm². Electrochemical impedance spectroscopy (EIS) was performed with a potentiostat/galvanostat (PGSTAT 30, Autolab, EcoChemie, the Netherlands) under illumination. The frequency range was explored from 0.01 Hz to 0.1 MHz. The applied bias voltage and ac amplitude were set at open-circuit voltage of DSSCs and 10 mV.

3 Results and discussion

Titanium (Ti) films were deposited on FTO substrates using DC magnetron sputtering. The typical SEM images of Titanium films are shown in Fig. 1. The substrate temperature for the deposition of Ti film plays an important role in controlling the adhesion and morphology of TiO₂ nanotube growth [9]. The sputter deposited films at 300 °C exhibit columnar structures as seen in the cross-sectional view of Ti films and surface of the Ti films is smooth and dense. The thickness of the Ti film is about 2 μm .

Mor et al. [10] have suggested that Ti anodization occurs as a result of a competition between electrochemical

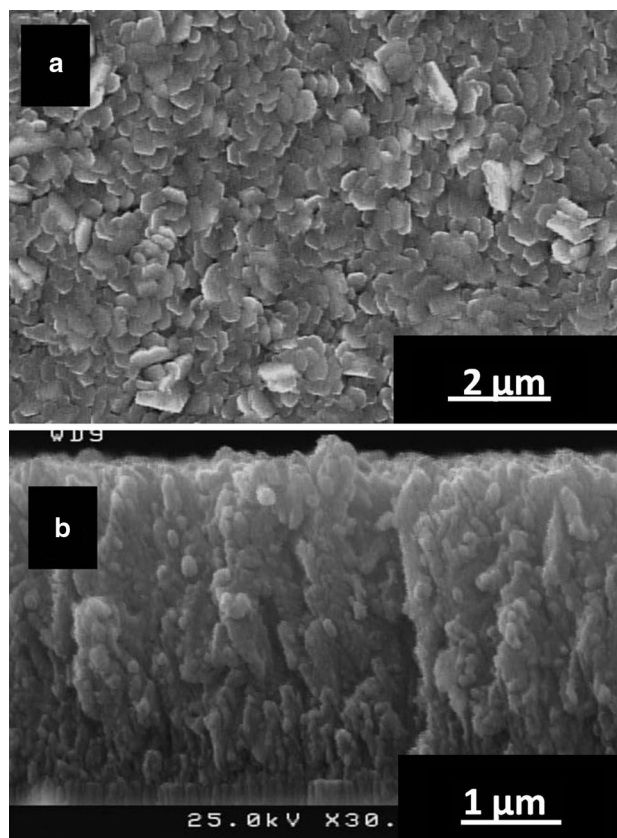
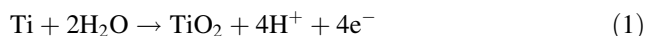


Fig. 1 FESEM images of Ti film sputtered on FTO coated glass substrate, **a** top view, **b** cross-sectional view

oxide formation and chemical dissolution of oxide by fluoride ions. A thin oxide barrier layer is initially formed by the reaction:



Next, pores are formed due to localized chemical dissolution of the oxide by F^- and formation of soluble $[\text{TiF}_6]^{2-}$ complex. This process occurs by the following reaction:

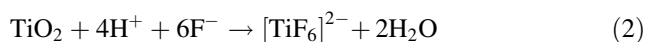


Figure 2 shows the current density versus time curve obtained during the anodization of Ti thin film at 50 V in 0.5 wt% NH_4F /ethylene glycol solution. The duration of anodization was about 18 min. At the beginning of the anodization process, the current rises and then drops drastically owing to the formation of compact oxide film at the electrolyte/metal interface, which elevates the resistance and reduces the current density. After a while, some cracks and narrow slits appear on the surface due to the chemical and field-assisted dissolution of the oxide layer, and then the current begins to rise gradually owing to the reduced oxide layer thickness and formation of TiO_2 nanotube layer. Finally, the current decreases again as the TiO_2 nanotubes become thicker and more resistive while the titanium film below the oxide layer becomes thinner. It has been reported that the anodization in the organic electrolyte produces very smooth curves without any fluctuations in current. It was due to the lower diffusivity and concentration of ions in the organic electrolyte [11].

FESEM images of the TiO_2 nanotube arrays grown on top of the FTO/glass substrate are shown in Fig. 3. From the top view (Fig. 3a), a compact nanoporous layer is visible on top of the TiO_2 NTs. Similar nanoporous layer after Ti anodization was reported in literatures [11, 12], and methods like sonication in diluted HCl or immersion into diluted HF solutions were proposed to remove it [13]. In

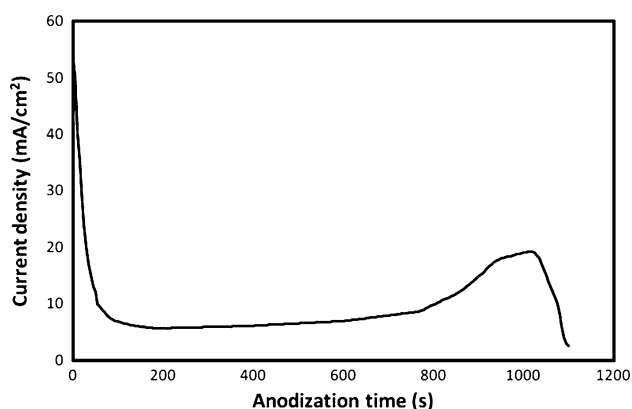


Fig. 2 Current density-time curve recorded during the anodization of Ti films at 50 V in 0.5 wt% NH_4F /ethylene glycol solution

the present study, the nanoporous top layer seems to be quite resistive to chemical dissolution and all attempts to remove it by sonication in dilute acid solution failed. Moreover, in case of using diluted HF, it is easy to damage TiO_2 NT layers and even detach them from the substrate. Also, some groups reported that the sputtering deposition parameters and crystallographic orientation of the Ti film play a significant role in determining whether porous or tubular structures were formed during the anodization process [14, 15].

Regular morphology of TiO_2 nanotube arrays are revealed in our study, as observed from bottom view of the anodized layer (Fig. 3c). Thus, we can conclude that ordered array of nanotubes are formed beneath this upper nanoporous layer. It can be seen from Fig. 3c that the resulting NTs have average pore size and wall thickness of about 70 and 30 nm, respectively. Cross-sectional view of FESEM images (Fig. 3b) shows that the thickness of TiO_2 NTs is about 4.8 μm . The tubes are 2.4 times longer than the thickness of the sputtered Ti film, showing little undesired dissolution of the metal in the electrolyte during anodization. Pilling–Bedworth ratio (“expansion factor”) of a TiO_2 grown film to an initial sputtered Ti film is reported to be close to 2.4–2.7 for the TiO_2 NTs anodization in viscous electrolyte [16]. Digital images in Fig. 3d clearly show the change of titanium sputtered on FTO/glass substrate after anodization. The anodized area becomes almost transparent after anodization.

The prepared TiO_2 NTs by Ti anodization are usually reported to be amorphous and can be crystallized by annealing which is desirable for electron transport [17, 18]. The phase structure of TiO_2 NTs was characterized by XRD measurements after annealing at 450 $^{\circ}\text{C}$. As shown in Fig. 4, annealed samples exhibited tetragonal anatase crystal phase TiO_2 (JCPDS No: 21-1272) with the (101) preferred orientation. Peaks at $2\theta = 25.3^{\circ}$, 37.9° , 48.4° and 54° corresponds to the planes (101), (103), (200) and (105), respectively. The peaks at $2\theta = 26.5^{\circ}$, 33.7° , 37.7° , 51.6° , 54.6° , 61.6° and 65.7° in the XRD pattern are attributed to SnO_2 peaks [JCPDS card no. 77-0452] which belong to FTO.

The current density–voltage curve of the DSSC, using annealed TiO_2 NT arrays as photoanode is shown in Fig. 5 and the photovoltaic characteristics are summarized in Table 1. The cell exhibited a short-circuit current density (J_{sc}) of 6.71 mA/cm^2 , an open circuit-voltage (V_{oc}) of 0.59 V and a fill factor (FF) of 0.50 with an overall conversion efficiency of 1.97 %.

Compared to the traditional high efficiency (>10 %) TiO_2 nanoparticle DSSCs [19, 20], the fabricated TiO_2 NT DSSC in this work showed lower power conversion efficiency. The major factor that limits the power conversion efficiency here is the low photocurrent due to limited thickness of TiO_2 layer. The J_{sc} increases with increasing

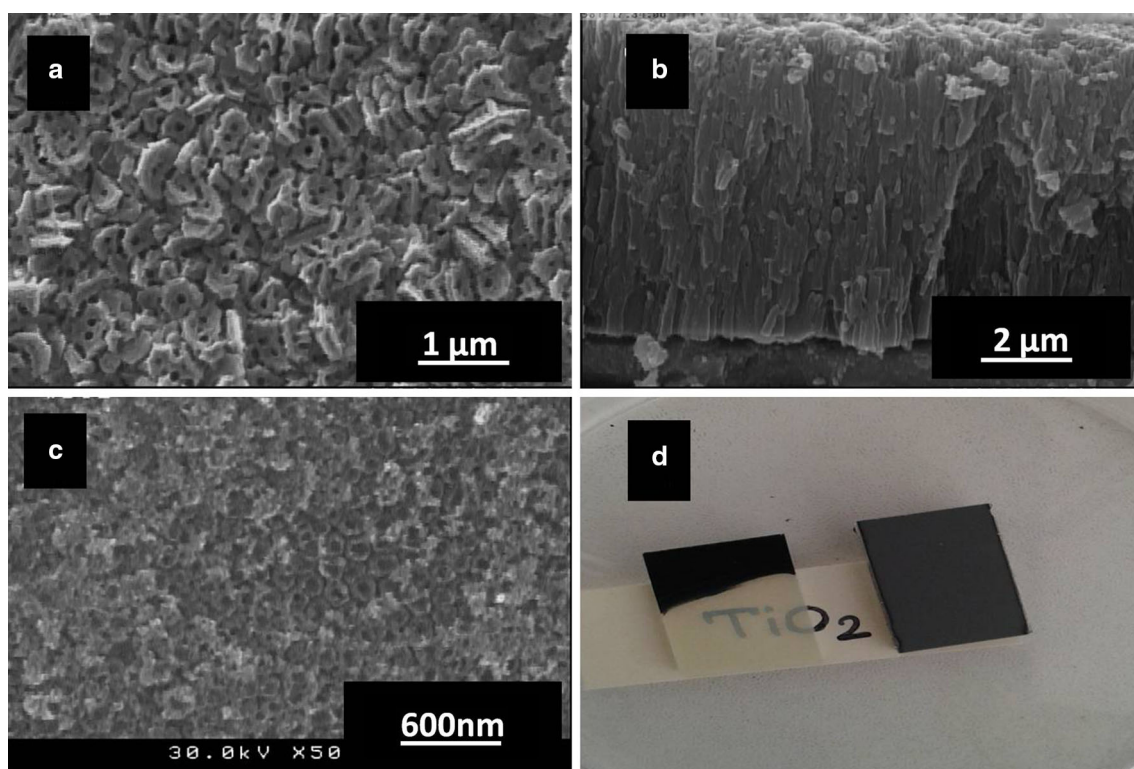


Fig. 3 FESEM images of titanium film anodized at 50 V in 0.5 wt% NH_4F /ethylene glycol solution: **a** top view, **b** cross-sectional view, **c** bottom of anodized layer and **d** digital images of Ti sputtered FTO glass and transparent TiO_2 nanotube sample after Ti anodization

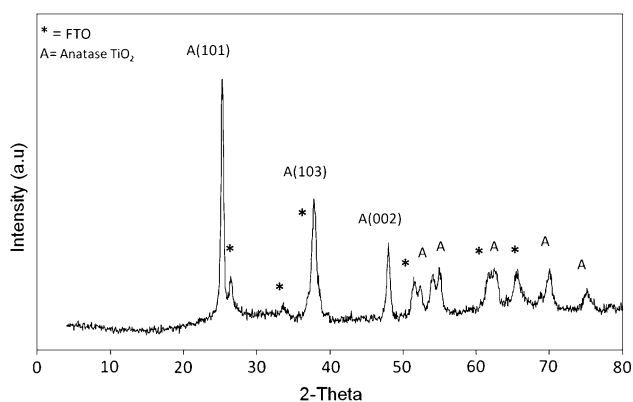


Fig. 4 XRD pattern of annealed TiO_2 nanotube sample fabricated in ethylene glycol electrolyte containing 0.5 wt% NH_4F and anodization voltage of 50 V

the NTs' length which can be possibly attributed to the increase in the number of adsorbed dye molecules, and therefore, a higher number of photogenerated electrons. Moreover, the long NTs would also improve the light-harvesting efficiency, which could also be a result of stronger light-scattering effects [5, 21]. However, it should be noted that further increase in the nanotube length may reduce the J_{sc} due to increase the photoanode thickness

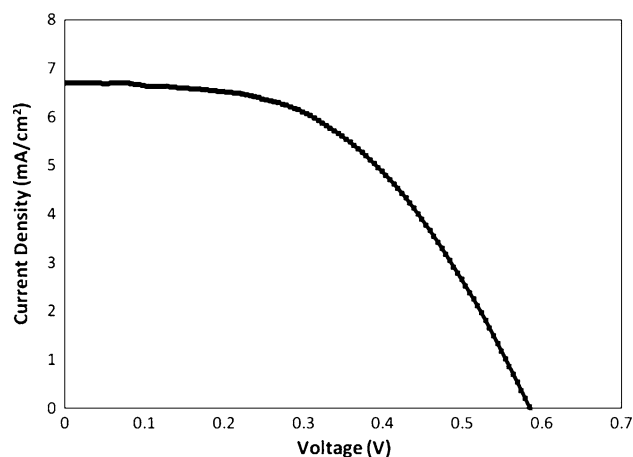


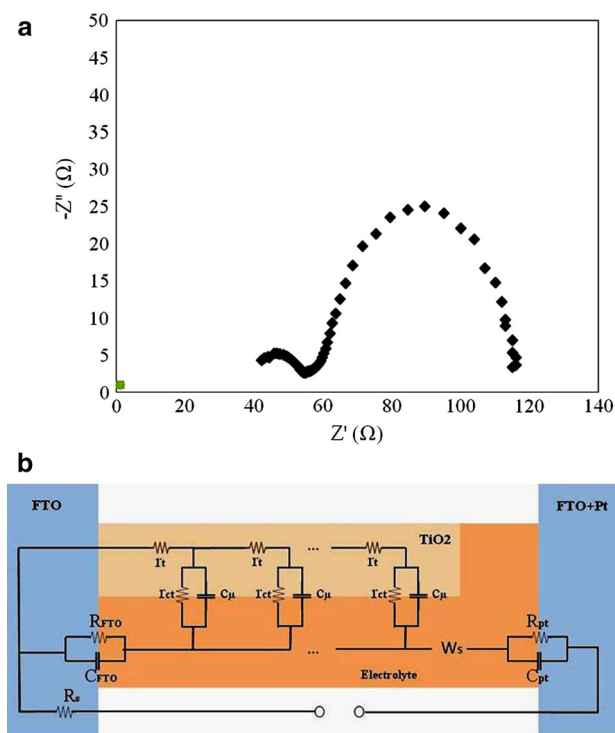
Fig. 5 Current density versus voltage curve of the DSSC, using the prepared TiO_2 nanotube sample as photoelectrode

beyond the electron diffusion length and hence increase the electron recombination [17].

Another factor that limits the DSSC efficiency is low fill factor which is reduced with increasing series resistance. Poor contact between the NTs and the FTO substrate is a reason of high series resistance. Modification of annealing step and TiCl_4 post-treatment of the NTs would improve

Table 1 Cell performances and electron transport properties of DSSC, using the prepared TiO₂ nanotube sample with thickness of 4.8 μm as photoelectrode

Cell performance				Electron transport properties					
V _{oc} (V)	J _{sc} (mA/cm ²)	FF	η (%)	R _t (Ω)	R _{ct} (Ω)	C _{μ} (F)	D _n (cm ² /s)	L _n (μm)	τ_n (ms)
0.59	6.71	0.5	1.97	18.87	55.03	1.25E−3	1.06E−5	8.54	68.7

**Fig. 6** **a** Impedance spectra of DSSC based on TiO₂ nanotube sample. **b** General transmission line model of DSSCs

the fill factor. In addition, J_{sc} can be enhanced by TiCl₄ post-treatment [20, 22].

EIS measurement was also applied to characterize the electron transport and recombination properties of DSSCs. Figure 6a shows typical Nyquist plot of the impedance data. A suggested equivalent circuit representing DSSC (Fig. 6b), which is proposed according to the diffusion-recombination model developed by Bisquert [23], is employed to fit the impedance spectra.

By modeling and fitting the EIS data of DSSCs, we can obtain the electron transport parameters in the photoanode, including the electron transport resistance $R_t = r_t L$ in the photoanode, the charge transfer resistance $R_{ct} = r_{ct} / L$ related to recombination of an electron at the TiO₂/electrolyte interface, and the chemical capacitance $C_\mu = c_\mu L$ of the semiconductor, where L refers to the film thickness. Moreover, the effective diffusion coefficient $D_n = L^2 / R_t C_\mu$ of an electron, the recombination lifetime $\tau_n = R_{ct} C_\mu$

and the effective electron diffusion length $L_n = \sqrt{D_n \tau_n}$ in the photoanode of the DSSCs were further estimated (Table 1).

From EIS measurement, it is found that the electron diffusion length (L_n) of NT based DSSC, which depends on both the τ_n and D_n , is around 8.6 μm (Table 1), which is higher than the thickness of the TiO₂ film (4.8 μm). However, Wang et al. [24] reported that the L_n of a DSSC needs to be at least three times the thickness of the TiO₂ film in order to collect most of the photogenerated electrons. Electron life time (τ_n) was obtained as high as 68.7 ms which is comparable with literature values for NT photoanodes [5].

Tsai et al. [25] reported the electron transport resistance of 19.2 Ω for the DSSC fabricated using 12.7 μm TiO₂ nanoparticle film as the photoanode. In this study, TiO₂ NT photoanodes with thickness of 4.8 μm showed lower transport resistance ($R_t = 18.87 \Omega$).

Furthermore, recombination resistant, R_{ct} , was obtained 55.03 Ω that is comparable with literature data [26], implying that recombination of electrons through the electrolyte is not the dominant effect limiting photovoltaic performance.

4 Conclusions

In summary, TiO₂ NT arrays with a thickness of 4.8 μm and a pore diameter of 70 nm were successfully grown on transparent conductive FTO substrates by anodizing the sputtered Ti films. The anodization was carried out under ethylene glycol based electrolyte containing 0.5 wt% NH₄F at a voltage of 50 V with the high ratio of the thickness of the anodic film to the thickness of the oxidized titanium layer (2.4). The as-grown NTs were amorphous and crystallize mainly in the anatase form by annealing at 450 $^{\circ}\text{C}$. Then the prepared sample was used as photoanode to assemble the DSSC, and the open circuit voltage of 0.59 V and a short circuit current density of 6.71 mA/cm² were obtained. The fill factor and the conversion efficiency were 0.50 and 1.97 %, respectively. The relatively low photocurrent is attributed to limited thickness of NTs. Electrochemical impedance spectroscopy (EIS) showed that the electron diffusion length (8.6 μm) was higher than

NTs' height. It was also observed that the electron transport resistance measured in NT DSSC was lower compared to the reported TiO₂ nanoparticle one.

Open Access This article is distributed under the terms of the Creative Commons Attribution 4.0 International License (<http://creativecommons.org/licenses/by/4.0/>), which permits unrestricted use, distribution, and reproduction in any medium, provided you give appropriate credit to the original author(s) and the source, provide a link to the Creative Commons license, and indicate if changes were made.

References

1. M. Adachi, Y. Murata, M. Harada, Y. Yoshikawa, *Chem. Lett.* **29**, 942 (2000)
2. D.-J. Yang, H. Park, S.-J. Cho, H.-G. Kim, W.-Y. Choi, *J. Phys. Chem. Solids* **69**, 1272 (2008)
3. G.K. Mor, O.K. Varghese, M. Paulose, K.G. Ong, C.A. Grimes, *Thin Solid Films* **496**, 42 (2006)
4. L. Cao, C. Wu, Q. Hu, T. Jin, B. Chi, J. Pu, L. Jian, *J. Am. Ceram. Soc.* **96**, 549 (2013)
5. K. Zhu, N.R. Neale, A. Miedaner, A.J. Frank, *Nano Lett.* **7**, 69 (2007)
6. D. Gong, C.A. Grimes, O.K. Varghese, W. Hu, R.S. Singh, Z. Chen, E.C. Dickey, *J. Mater. Res.* **16**, 3331 (2001)
7. K. Shankar, G.K. Mor, H.E. Prakasam, S. Yoriya, M. Paulose, O.K. Varghese, C.A. Grimes, *Nanotechnology* **18**, 65707 (2007)
8. Y. Wang, H. Yang, Y. Liu, H. Wang, H. Shen, J. Yan, H. Xu, *Prog. Photovoltaics Res. Appl.* **18**, 285 (2010)
9. X. Chen, J.-S. Wang, H.-Y. Li, K.-L. Huang, G.-S. Sun, *Res. Chem. Intermed.* **37**, 441 (2011)
10. G.K. Mor, O.K. Varghese, M. Paulose, N. Mukherjee, C.A. Grimes, *J. Mater. Res.* **18**, 2588 (2003)
11. D.-J. Yang, H.-G. Kim, S.-J. Cho, W.-Y. Choi, *Mater. Lett.* **62**, 775 (2008)
12. A.Z. Sadek, H. Zheng, K. Latham, W. Wlodarski, K. Kalantar-Zadeh, *Langmuir* **25**, 509 (2008)
13. D. Kim, A. Ghicov, P. Schmuki, *Electrochem. Commun.* **10**, 1835 (2008)
14. K. Kalantar-Zadeh, A.Z. Sadek, H. Zheng, J.G. Partridge, D.G. McCulloch, Y.X. Li, X.F. Yu, W. Wlodarski, *Appl. Surf. Sci.* **256**, 120 (2009)
15. K.N. Chappanda, Y.R. Smith, L.W. Rieth, P. Tathireddy, M. Misra, S.K. Mohanty, *Nanotechnology. IEEE Trans.* **14**, 18 (2015)
16. S. Berger, J. Kunze, P. Schmuki, D. LeClere, A.T. Valota, P. Skeldon, G.E. Thompson, *Electrochim. Acta* **54**, 5942 (2009)
17. B.-X. Lei, J.-Y. Liao, R. Zhang, J. Wang, C.-Y. Su, D.-B. Kuang, *J. Phys. Chem. C* **114**, 15228 (2010)
18. H. Zheng, A.Z. Sadek, M. Breedon, D. Yao, K. Latham, J. du Plessis, K. Kalantar-Zadeh, *Electrochem. Commun.* **11**, 1308 (2009)
19. M.K. Nazeeruddin, F. De Angelis, S. Fantacci, A. Selloni, G. Viscardi, P. Liska, S. Ito, B. Takeru, M. Grätzel, *J. Am. Chem. Soc.* **127**, 16835 (2005)
20. O.K. Varghese, M. Paulose, C.A. Grimes, *Nat. Nanotechnol.* **4**, 592 (2009)
21. R. Soleimanzadeh, M. Kolahdouz, M.A. Charsooghi, Z. Kolahdouz, K. Zhang, *Appl. Phys. Lett.* **106**, 231102 (2015)
22. G.K. Mor, K. Shankar, M. Paulose, O.K. Varghese, C.A. Grimes, *Nano Lett.* **6**, 215 (2006)
23. F. Fabregat-Santiago, J. Bisquert, G. Garcia-Belmonte, G. Boschloo, A. Hagfeldt, *Sol. Energy Mater. Sol. Cells* **87**, 117 (2005)
24. H. Wang, L.M. Peter, *J. Phys. Chem. C* **113**, 18125 (2009)
25. J.K. Tsai, W.D. Hsu, T.C. Wu, T.H. Meen, W.J. Chong, *Nanoscale Res. Lett.* **8**, 1 (2013)
26. T. Stergiopoulos, A. Valota, V. Likodimos, T. Spiliotis, D. Niarchos, P. Skeldon, G.E. Thompson, P. Falaras, *Nanotechnology* **20**, 365601 (2009)